Proceedings of ASME Turbo Expo 2011
GT2011
June 6-10, 2011, Vancouver, British Columbia, Canada

GT2011-46160

SWIRL-ENHANCED INTERNAL COOLING OF TURBINE BLADES – PART 1 RADIAL FLOW ENTRY

Del Segura and Sumanta Acharya

Louisiana State University
Turbine Innovation and Energy Research (TIER) Center
Department of Mechanical Engineering
Baton Rouge, LA 70803, U.S.A.

ABSTRACT

Heat transfer results for a given slot shaped channel with a 3:1 aspect ratio and jets issuing from side walls are presented. Two different jet configurations are used as a means to enhance turbulence in the main flow stream. The Reynolds numbers investigated range from 10,000 to 50,000 and are based on the mean velocity of the fluid at the channel inlet for the slot shaped channel without enhancement, or when swirl-jets are used, the equivalent mass flow rates at the exit of the main channel. Blowing Ratios, defined as the mean side jet velocity verses the mean main channel velocity, ranged from 8.6 to 30.2. This heat transfer enhancement strategy has proven to be effective in round channels.

A transient technique combined with Duhamel's superposition theorem was used to obtain the heat transfer coefficient distributions. Narrow-band liquid crystals were used to map the transient surface temperatures and were combined with thermocouples that measured the center-line air temperatures along the flow path in the main channel. The results of the passage with jet enhancements were compared to the smooth slot channel, without any type of heat transfer enhancements. The tests results reported in this paper show mean heat transfer enhancement values ($Nu/Nu_{o\ smooth}$) greater than 4.2 and low normalized friction factors. Thermal performance factors (OTP) ranged from 1.55-3.69 for the various configurations studied. These results show significant improvements over other types of heat transfer enhancement methods currently used in the mid-span section of turbine blades.

INTRODUCTION

One of the most critical problems that still exist in gas turbine engines is the ability to achieve efficient turbine blade cooling using a simple, inexpensive and reliable cooling design. The quest to achieve improvements in performance and fuel economy drive the need to develop new and innovative turbine blade internal cooling strategies.

Current turbine inlet temperatures (~1500 ^{0}C) exceed the limits of blade material (~1000 ^{0}C) and must be cooled to avoid catastrophic failures. A portion of the compressor air is bypassed, redirected into passages in the turbine blade where this cooler air (~650 ^{0}C) reduces the external blade temperature to acceptable levels. As shown in figure 1, the common configurations for airfoil cooling include ribs, pin-fins, impingement jets, and film cooling holes [1]. These cooling strategies have fared well over the last few decades, but at a cost to the overall operating efficiency due to the amount of compressor bypass air needed. Recent studies have indicated that marked improvements to effective heat transfer can be gained by utilizing swirl/cyclone motion in the internal passages [2-3]. These studies used round channels with rectangular jet slots and reported local heat transfer enhancements of 4-5. These values may yield as much as a 25% improvement over a similarly designed passage with ribbed

turbulators. However, for heat transfer, a rather limited number of configurations have been studied with swirl and have been generally limited to round tubes.

Swirling flows in channels provide the benefits of longer residence times, higher turbulence levels and can be combined with trip strips. A specific variant of this technique is the concept of lattice cooling [4-7] where a lattice network is used to increase the flow path, and combined with the associated impingement and trip-strips produced high heat transfer coefficients. Local values of Nu/Nu_o in the impingement areas are in the range of 6-10. A key drawback with this approach is the higher pressure-drop penalty and the added weight of the lattice. Therefore strategies that combine swirl and impingement with relative lower pressure-drop penalty are still sought.

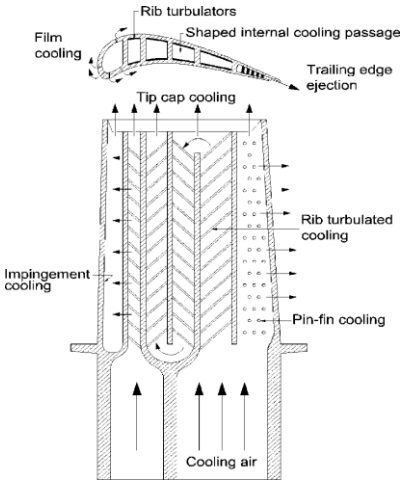

FIGURE 1: CROSS SECTION OF TYPICAL TURBINE BLADE WITH INTERNAL COOLING [1]

The current mainstream internal cooling strategies add ribs to a smooth channel to induce vortices and flow reattachment as the fluid passes over the rib.

Wang, et-al [8] performed a detailed study of various rib shapes in a square ducts with a rib pitch to rib height ratios varying from 8 to 15 and rib height to hydraulic diameter value of 0.1. The range of Reynolds numbers tested was 8,000 to 20,000. The highest Nu/Nu_o values occurred with the rib pitch to rib height ratio of 12 at Re=20k. Overall thermal performance (OTP) values were not presented. Taslim, et-al [9] tested several different rib configurations and determined a rib height to hydraulic diameter value of 0.125 provided the best results. They presented overall thermal performance (OTP) values as high as 1.9 at Re=10k to 1.5 at Re=25k. Many other studies show similar findings. The rib pitch and rib heights, as related to hydraulic diameters in these studies were used as guidelines in determining the jet diameters and jet pitch used in this study.

Kurtbaş, et-al [10] studied the effects of inducing swirl into a smooth channel by using flow directed swirl generator nozzles at the inlet of a round channel with uniform heat flux. Cone insert angles of 30^o, 45^o, and 60^o and flow director angles of 30^o, 60^o, and 90^o were examined. Reynolds numbers of 9,400 to 35,000 were used throughout the various test performed. Pressure drop was also measured and finally an overall thermal performance value was determined. The results yielded overall thermal performance (OTP) values ranging from 2.2 at Re=10k to 1.2 at Re=35k.

High heat transfer enhancement values were noted in studies utilizing swirl/cyclone motion in round internal passages with rectangular shaped side jets [11]. Local thermal performance values (OTP) of 4-5 are reported, which yield substantial improvements when compared to similar passages with more conventional types of heat transfer enhancements. There have been a limited number of publications with other configurations utilizing swirl enhancements.

In the present paper, a unique strategy for generating a swirling flow in internal passages is studied, and measurements are reported for the normalized Nusselt number and overall thermal performance. The goal is to find strategy that will produce high heat transfer enhancements without significant pressure drop penalty. Although the outer jet supply channels play in integral role in this design, the heat transfer enhancement is these channels are not considered in this study. In a real world practical application, the outer jet supply channels would have their own heat transfer enhancement strategy.

NOMENCLATURE

A	Cross section area, m^2
AR	Aspect Ratio, a/b
a	Width of slot channel, *mm*
b	Height of slot channel, *mm*
BR	Blowing Ratio
BFM	Back Flow Margin
d	Jet hole diameter, *mm*
d_h	Channel Hydraulic Diameter, *m*
f	Friction Factor in the Channel
f_o	Friction Factor in a smooth round pipe
h	Convection Heat Transfer Coefficient, $W/m^2 K$
k	Coefficient of thermal conductivity, $W/m K$
L	Channel Length, *mm*
$\dot{m}$	Mass flow rate, *(kg/s)*
Nu	Nusselt Number
Nu_o	Nusselt Number for a smooth round pipe
p	Pitch, *mm*
Pr	Prandtl Number

P Pressure, *Pa*
P_m Pressure, Main Channel, *Pa*
P_o Pressure, Outer Jet Supply Channel, *Pa*
ΔP Total Pressure Loss in Test Piece
Re Reynolds Number
t time, *s*
T_w Wall temperature, *K*
T_i Initial temperature, *K*
$\Delta T_{m,i}$ Temperature difference between each time step, *s*
T_m Fluid temperature, K
U_m Mean Velocity, *m/s*

Greek

α Coefficient of thermal diffusivity, m/s^2
ρ Density, kg/m^3
τ Time step for each temperature step, *s*

CONFIGURATIONS STUDIED

A 3:1 AR single passage channel with a hydraulic diameter, d_h, of 0.0248m and an L/d_h of 8.7 is chosen for this study.

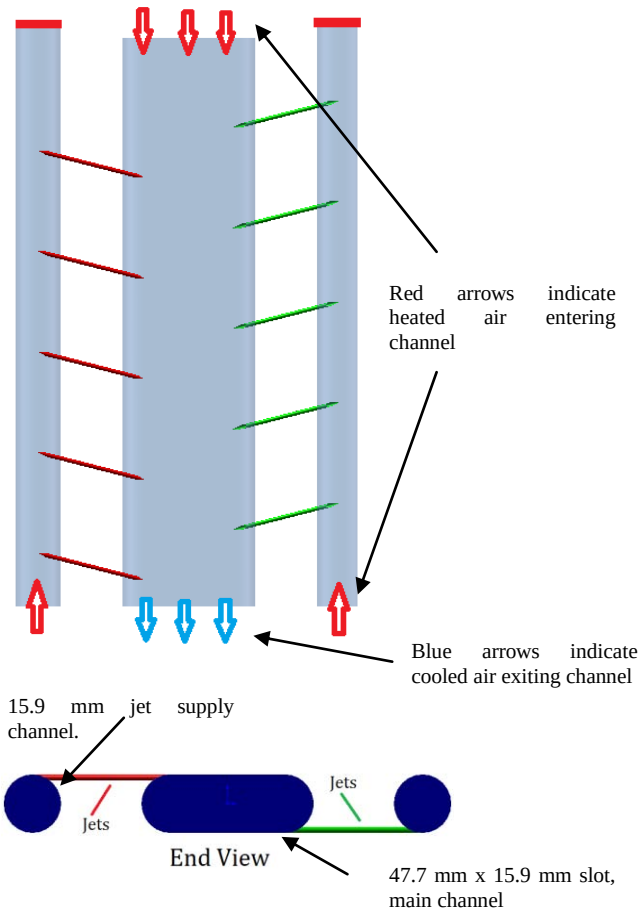

FIGURE 2: TOP & END VIEW OF TYPICAL FLUID PASSAGES.

The configurations investigated to enhance heat transfer include fluidic-swirl-generation strategies where swirl is generated by introducing tangential jets along the side walls of the main coolant passage. Figure 2 shows the generic flow path of the fluid, with the end view showing the location of the round jets tangent to the walls of the walls of the main channel.

The two fluidic swirl-generation configurations are shown in figure 3, where the different configurations are shown and labeled as A and B.

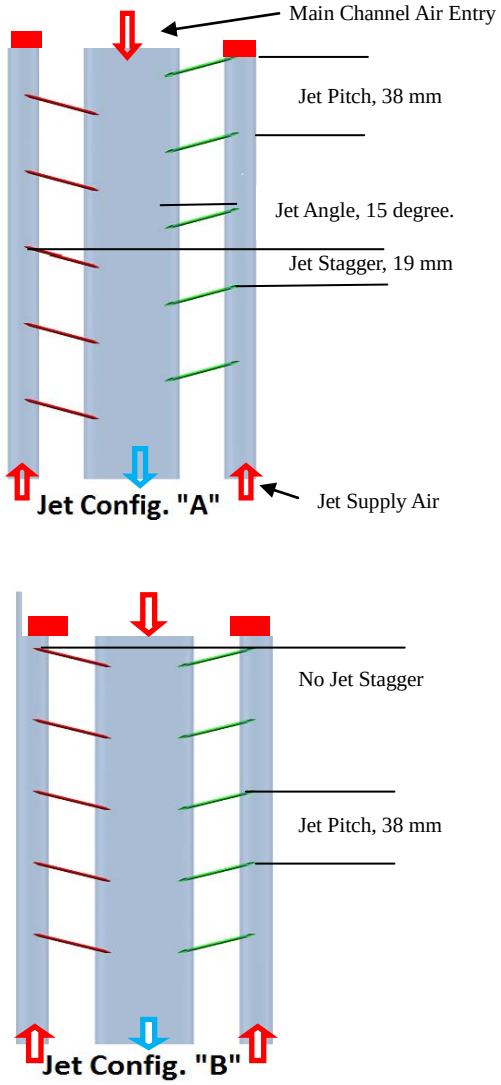

FIGURE 3: JET CONFIGURATION SCHEMES

In both configurations, air enters the main channel radially through a 3:1 AR slot shaped passage as well as through tangential side jets introduced through several holes placed axially along the neighboring (side) channels. Flow

through the side-channels feeding the jet-holes was opposite to the main channel flow direction. The side-jets are introduced tangential to the main flow to produce a swirling motion, and are oriented at a 15 degree angle to the streamwise direction. In addition to the swirl, the jets are angled towards the main flow to generate counter-shear and associated turbulence. In figure 2, the red and green lines indicate the location of the jets entering the main channel. The pitch and offset of the jets are described in detail in the experiments section. The tangential jet from the left is introduced along the top surface of the channel while the tangential jet from the right is introduced at the bottom of the channel. The two configurations differ in the relative offset between the left and right jets. The entrance and exit to the main channel have a 12.5 mm radius. A transparent CAD model of the test piece is shown in Figure 4.

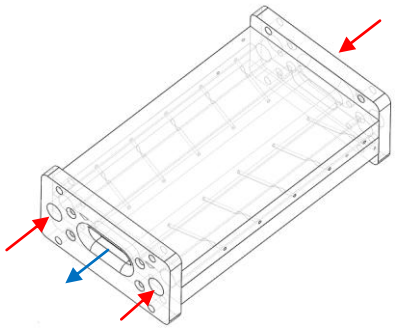

FIGURE 4: TRANSPARENT CAD MODEL OF THE TEST PIECE.

A channel-average blowing ratio, jet velocity to main channel velocity, was varied in each test. The average blowing ratio was calculated based on the measured mass flow rates and pressures in the main channel and the side channels, and is an average value across all the jet-holes. The individual jet-blowing ratio may vary from hole to hole depending on the pressure drop across the holes.

The minimum blowing ratio selected was a value that created a high enough jet exit velocity to ensure that the jet penetrated the main flow field to the other side, and potentially created an impingement effect. As a basis for comparison and normalization, an equivalent smooth-channel case with no swirl-enhancement was considered, with a mass flow rate equivalent to the sum of the main and side channel mass flow rates exiting the main channel for the swirl-enhanced cases. The total mass flow rate combined with the hydraulic diameter of the main channel was used to define the Reynolds number of the flow. The results of all tests presented in this paper are compared (normalized) with the non-enhanced smooth channel designated by $Nu_{o\ smooth}$.

In most of the color contour plots shown in this paper, it was necessary to use different scales to accent notable heat transfer regions. In order to more easily differentiate various configurations line plots of the average values are also presented.

EXPERIMENTS

Experimental Apparatus

A simulated clear polycarbonate airfoil was built that incorporates a strategy for inducing swirl motion in the internal passages of an airfoil. The main cooling channel is slot shaped with an aspect ratio of 3:1, with a height of 15.9 mm and a width of 47.6 mm. The overall length of the slot channel is 216 mm, not including a 12.5 mm radiused entry and 12.5mm radiused exit portion of the channel.

The side-jets that produce swirl are fed through outer passages that run parallel to the main slot shaped channel. These passages are 15.9 mm in diameter and the diameter of the jet at the entrance to the main channel is 1.6 mm. The flow into the jet supply channels was not through flow and could only exit through the jets (see figure 2). The jets were spaced 38 mm apart along one side. In configuration "A", the jets located on the opposite wall were offset by 19 mm relative to each other. In configuration "B" the jets were aligned (no offset) relative to each other along both walls of the main channel. The red and green lines indicate jet locations and sides. In each case the temperature at the entry of the respective channels at the beginning of the tests was maintained within two degrees Celsius of each other.

Initial static testing was performed using 25 thermocouples strategically placed in the passage of the channel. A smooth channel with no swirl inducement strategies was tested first, and the results of normalized heat transfer enhancement and pressure losses were used to compare against all tests with swirl enhancements. Testing with thermocouples as well as liquid crystal techniques will provide a more detailed account of heat transfer enhancement in the passage.

Heated air enters the test piece via a long diffuser section through a 12.5 mm radiused entry and exits the single flow slot shaped channel in an identical fashion. Upon exiting the channel the air is routed through a small plenum, then finally exits through two 18 mm holes to the atmosphere. The main channel inner walls are coated with a specially prepared thermochromic liquid crystal (TLC) substance which turns green at a nominal temperature of 35^0C. Two thin film thermocouples are attached to the walls, one near the entry and one near the exit of the main channel. These will be used to confirm the accuracy of the TLC. Five fine wire thermocouples are placed, equally spaced, in the center of the main channel flow stream. The thermocouples are wired directly to a Labview thermocouple data acquisition system. The thermocouples have a resolution of 20 Hz and the data acquisition system is set to read thermocouple data at 15 Hz.

Two Canon SD430 wireless cameras are securely mounted on each side of the test piece. The cameras are set to record video images at 15 Hz. The thermocouple data acquisition system and the video cameras are synchronized via cold cathode fluorescent lamps (CCFL) that are used to illuminate the TLC and are triggered by a switch attached to one of the two air bypass valves.

Prior to the start of a test, heated air is allowed to bypass the test section. Once the bypassed heated air temperature has stabilized at approximately 80^{o} C preparations for the start of a test begins. The test piece is also maintained at room temperature for an extended period prior to the start of a test to ensure a uniform initial temperature.

Two separate heaters were used. One heater was used to heat air entering the main slot channel and the other was used to heat air entering the two outer jet supply channels. Two separate flow meters were used to control the mass flow rate of air entering each channel. As stated, the combined mass flow rate at the exit of the test piece is used to determine an equivalent Reynolds number for comparison with tests that do not utilize jets. The heated air from each heater is bypassed and allowed to stabilize prior to the start of a test. It is desirable to have the air entering each channel to be the same throughout the entire test.

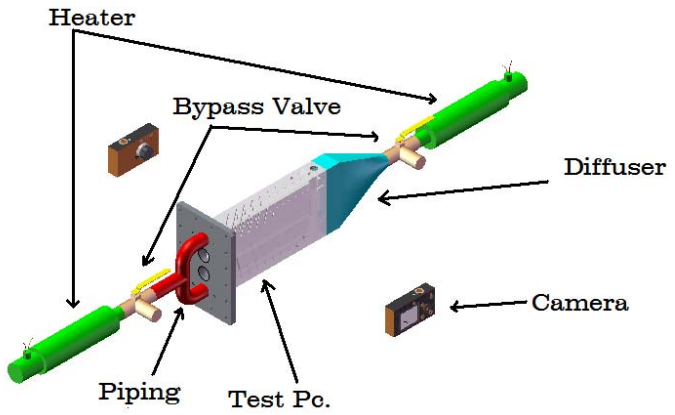

FIGURE5: BASIC LAYOUT OF TEST APPARATUS

This is quite a difficult task due to heat losses in the apparatus being somewhat different as the heated air travels from the individual heaters to the channel inlets. Thermocouples located at the entry of each channel monitor the temperature of the air entering the channel. Temperature differences of two degrees Celsius between the main and outer channel inlets were considered to be in the acceptable range for testing. Repeat testing using inlet air temperature differences as high as ten degrees Celsius were performed to better understand this effect.

To begin a test, the thermocouple data acquisition system is activated and the cameras begin recording. Then a bypass valves are closed allowing heated air to enter the test piece. Video images and thermocouple temperature readings are stored for post processing. The basic layout of the test apparatus is shown in figure 5.

Heat Transfer Coefficients

The local heat transfer coefficients across a liquid crystal coated target surface can be obtained using the 1-D transient heat conduction model of a semi-infinite solid with a convective boundary condition as given by:

$$\frac{\partial^2 T}{\partial x^2} = \frac{1}{\alpha}\frac{\partial T}{\partial t} \tag{1}$$

with boundary and initial conditions:

$$\begin{aligned} &\text{at } t = 0, T = T_i \\ &\text{at } x = 0, -k\frac{\partial T}{\partial x} = h(T_w - T_m) \\ &\text{at } x \to \infty, T = T_i \end{aligned} \tag{2}$$

where h is the surface heat transfer coefficient, T_w is the time-varying wall surface temperature and T_m is the time-varying local bulk (for internal flows) temperature. This is measured in the present work using suspended centerline thermocouples at several axial locations. These suspended thermocouples acquire temperature changes throughout each test. The data is used to produce a curve fit of the centerline temperatures vs. time along the entire main channel. The temperature vs. time equation is then associated with each column of pixels in the video image. Therefore, each column of pixels (flow stream is along rows) has an associated time vs. temperature array of data.

The solution for the surface temperature response with time is:

$$\frac{T_w - T_i}{T_\infty - T_i} = 1 - exp\left(\frac{h^2\,\alpha t}{k^2}\right) erfc\left(\frac{h\sqrt{\alpha t}}{k}\right) \tag{3}$$

A single transient test using the liquid crystal method described earlier is used. Each pixel value is examined for its peak in local intensity. The intensity value is used in conjunction with a specifically written MATLAB program to determine the corresponding time and bulk/centerline

temperature. By measuring the corresponding time required for the surface temperature to reach the TLC specified value, the local heat transfer coefficient can be determined.

The 1D semi-infinite solid assumption must be satisfied. In order to satisfy the semi-infinite assumption, the transient temperature must not penetrate through the thickness of the polycarbonate during the test duration. This is achieved by using a sufficiently thick test piece of low thermal conductivity and diffusivity (0.201 W/mK and 0.1046 $x10^{-6}$ m^2/s for polycarbonate respectively). For the one-dimensional heat transfer assumption to be satisfied, conduction should only occur normal to the surface with all lateral conduction effects neglected. The test piece may actually experience some lateral conduction, but it is assumed that the dominant temperature gradient is in the direction perpendicular to the surface, and lateral effects are negligible.

Although the initial temperature of the polycarbonate is uniform at ambient temperature, the incoming fluid temperature is higher and not a linear step increase. This is accounted for through the modification of the previous equation by Duhamel's superposition theorem, which represents the temperature change as a series of steps described by:

$$T - T_i = \sum_{i=1}^{N} \left[1 - exp\left(\frac{h^2}{k^2}\,\alpha(t-\tau_i)\right) erfc\left(\frac{h}{k}\sqrt{\alpha(t-\tau_i)}\right) \right] \Delta T_{m,i} \quad (4)$$

where τ is the time step for each temperature step, $\Delta T_{m,i}$ is the temperature difference between each temperature step and the initial temperature, T_i. α,and k are characteristics of the polycarbonate plate. In the cases where heat transfer enhancements using jets are incorporated, the air temperature at the entry of the main channel and the jet channel at the beginning of the tests were maintained within two degrees Celsius. The temperature of the fluid exiting the jets as expansion occurred is not known, but is assumed to be taken into account when the main channel centerline temperature vs. time data is obtained.

Pressure Tests

A pressure tap is located at each end of the main channel, and in the case of air flowing through the jet supply channels, additional pressure taps are located at each end of the outer jet channels (see figure 6). In order to obtain accurate and consistent results, pressure measurements were taken during steady state adiabatic tests.

Flow meters were positioned before the heaters each supply channel. The mass flow rate at the exit of each flow meter and pressure, temperature, and cross section area at the entry of each channel was used to determine velocities, densities, and associated Reynolds numbers, where applicable.

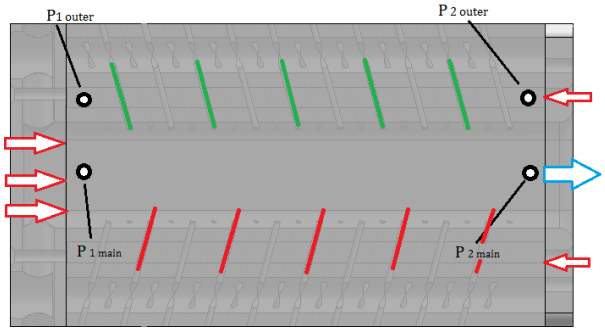

FIGURE 6: PRESSURE TAP LOCATIONS USED FOR PRESSURE LOSS CALCULATIONS.

Pressure drops along the main channel and outer channels are recorded and used to determine friction losses. The following equation is used to determine friction loss in each channel:

$$f = 2\, d_h \frac{\Delta P}{L \rho U^2} \quad (5)$$

Velocities are calculated based on flow rates and channel cross section area. The friction losses in each channel are proportional to one over the square of the velocity as determined by the mass flow rate. When testing with jet enhancements the mass flow into each channel can be used to determine the total combined friction loss by using the following equation for friction loss in parallel flow:

$$1/\sqrt{f_{total}} = \frac{1}{\sqrt{f_1}} + \frac{1}{\sqrt{f_2}} + \frac{1}{\sqrt{f_3}} \quad (6)$$

where f_1 is the friction loss in the main channel and f_2 and f_3 are the losses in the two outer jet supply channels. Friction losses in the actual jets are not taken into consideration.

When jet configurations were used the combined overall mass flow rates were used to compare the plain smooth channel (no enhancements) to that of the jet enhanced channel. As an example, Table 1 below shows the mass flow rates when jet configurations "A" or "B" were used along with a 17.5:1 blowing ratio. In this case, the percentage of mass flow rate through the jets ranged from 23% to 34%. The ratio of mass flow rates varied with each blowing ratio, with high blowing ratio tests having as much as 45% of the total mass flow entering the main channel through the side jets.

	Mass Flow Rate (kg/s)	
Reynolds Number	Main	Outer (Both)
10,000	0.00402	0.00140
25,000	0.00825	0.00531
40,000	0.01658	0.00507
50,000	0.02085	0.00619

TABLE 1: MASS FLOW RATES FOR JET CONFIG. "A" AND "B" w/ 17.5:1 BLOWING RATIO

In order for these configurations to work in a practical environment there must exists a pressure differential between the flow exiting the turbine blade, usually through film cooling holes, and the local pressure outside of the blade. Typically, a 4% to 7% pressure loss can be expected from the exit of the compressor section to the entry of the turbine blade. The configuration studied can only be useful if the pressure losses in the blade can are such that the exiting air is at a higher pressure than the pressure on the exterior of the blade. The high pressure losses associated with this design must not exceed the limitation of the engine. A safety margin must be established to prevent high temperature combustion gases from entering the interior of the blade. The concept of Back Flow Margin (BFM) is shown in Equation 7, where P_{int} is the internal pressure at the air exit point and P_{ext} is the external pressure at the same location. A typical value of 20-30% margin must be maintained and can differ according to the location on the blade.

$$\%BFM = \frac{P_{int} - P_{ext}}{P_{ext}} * 100\% \qquad (7)$$

To further clarify this in the context of the design presented, if the compressor exit pressure was 1035 kPa and there was a 7% pressure loss at the entry of the turbine (963 kPa) the pressure of the air leaving the internal cooling passages must be ~25% greater than the external pressure (963 kPa) at the point of exit. The actual pressure varies greatly on the turbine blade on the pressure and suction side, with the suction side pressure lower. Therefore, the amount of pressure loss in the internal passages is limited by the difference between the compressor exit pressure and the local pressure at the exit of the blade.

Pressure taps located at or near the entry and exit of the main channel as well as the entry and exit of the jet channels were used to determine the differential gauge pressure at each jet. As an example, the values for a blowing ratio of 17.5:1 are shown in Table 2 and were calculated based on the actual jet locations with the test piece set up in configuration "A". The "B" configuration showed similar results. A ~10-12% pressure drop exists between the first and last jet. This was typical throughout the range of blowing ratios. The pressure at the exit of the main channel remained slightly above atmospheric in all tests.

	$P_o - P_m$ (Pa)			
Jet Position	Re ~10k	Re ~25k	Re ~40k	Re~50k
1 (Main Channel Entry)	11231	35529	60621	65547
2	10857	34562	59429	63659
3	10477	33582	57739	61969
4	10098	32605	56049	60183
5 (Main Channel Exit)	9716	31622	54358	58394
Max. Delta P (kPa)	1515	3907	6263	7154

TABLE 2: PRESSURE BETWEEN OUTER (P_o) AND MAIN CHANNEL (P_m) AT VARIOUS JET LOCATIONS, CONFIGURATION "A" w/ 17.5:1 BLOWING RATIO

Experimental Uncertainty and Error

An accurate assessment of uncertainty in liquid crystal measurement of heat transfer coefficients is essential because many factors affect the TLC results. A large number of studies have concluded that a properly performed test yields mean uncertainly of up to 11.0% for values of h, and up to 9% for temperatures. Smith [12], et al, compiled a table summarizing uncertainty studies of h and T when narrow band TLC methods were used. Thermocouple accuracy and repeatability are large contributors to uncertainty as well as illumination spectral effects. The wall mounted thermocouples were used to compensate for this effect and resulted in a 0.2° C temperature correction.

Based on the methodology discussed by Smith [12] and the actual measurements taken, heat transfer values typically were repeatable within 3% - 5% for tests with Reynolds numbers up to 25,000 and blowing ratios below 20. The repeatability values increased to as high as 8% for higher Reynolds numbers and/or higher blowing ratios. As reported in the literature, the uncertainties in Nusselt numbers are approximately 10%. The uncertainty of the Nusselt numbers directly trends with the uncertainty of the heat transfer coefficients.

RESULTS AND DISCUSSION

Overall Heat Transfer and Friction

It is hypothesized that the angle and location of the jets provide several positive heat transfer effects. The high velocity

air issuing from the jets placed tangent to the walls of the main channel creates a high-shear flow phenomenon as the air travels along the walls of the main channel. High-shear can potentially lead to high heat transfer regions.

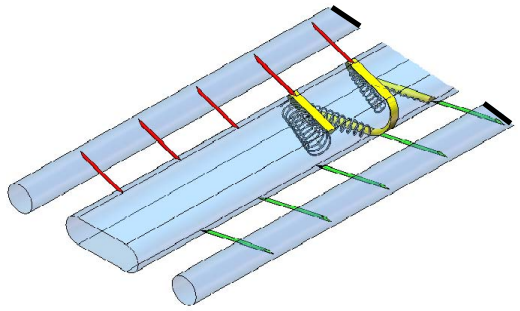

FIGURE 7: CONCEPT OF SWIRL AND TUMBLE CREATED BY ANGLED JETS ON EACH SIDE OF SLOT SHAPED CHANNEL.

The position of the jets in configuration "A" is such that the high velocity side-jet flow continues across the main channel, and proceeds around the end walls of the slot shaped channel. This jet flow encounters the high velocity jet stream exiting the succeeding jet on the opposite wall. It is hypothesized that the angle and location of the jets provide several positive heat transfer effects as the high velocity jet flow proceeds down the main channel along a pseudo-helical path. Additionally, when the lower velocity main channel air engages the high velocity jets in cross flow, the low velocity main channel air tumbles over the high velocity jets which act as pseudo-helical trip strips. The turbulence intensity grows as the main channel air proceeds along the flow path. Figure 7 shows this postulated phenomenon as increasing spirals attached to the imaginary helical strips created by the high velocity jets. Depending on the jet pitch, jet velocity, and main channel velocity, the location of the reattachment and recirculation regions will change. The results presented by Wang, et-al [8] clearly show this phenomenon. There exists an ideal combination of jet pitch, jet velocity, jet diameter, and blowing ratio that will maximize the local heat transfer enhancement. Because of the high turbulence occurring at each pair of jets and the increasing mass flow entering the main channel, the succeeding pair of jets encounter a different flow regime than the prior pair of jets. As a result, the local heat transfer enhancements can vary greatly as the flow proceeds from the main channel entry to the main channel exit. A much different combination of these parameters will maximize the overall heat transfer enhancement of the entire channel. Jet configuration "B", having aligned jets (see Figure 3), presents a completely different flow regime, but the same parameters can be varied to maximize local and overall heat transfer enhancement. Flow visualization studies were not performed to confirm the hypothesis.

While the flow paths used in this study may not directly translate to an actual turbine blade flow path, the concept of swirl and tumble used in this study has not been studied in detail in the past and can be a spring board to more detailed studies using flow path configurations used in actual turbine blades. The heat transfer characteristics of the round jet supply channels are not considered in this study.

The initial tests were performed with a smooth slot shaped channel with no heat transfer enhancements. The results of these tests showed heat transfer coefficients similar to the standard smooth pipe results noted by the Dittus-Boelter equation near the exit of the channel and somewhat higher values near the entrance of the channel, due to entry effect. The mean values of the heat transfer coefficient (h) and Nusselt number (Nu) over the entire channel were used as the standard for the remainder of testing. Thus, all references to Nu in this paper are listed as $Nu/Nu_{o\ smooth}$.

Values of mean $Nu/Nu_{o\ smooth}$ vs. Reynolds numbers for one side of the main channel and for all blowing ratios of jet configuration "A" are shown in figure 8 and for jet configuration "B" in figure 9. The results show the effectiveness of the jet configurations are extremely high ($Nu/Nu_{o\ smooth} \sim 4$) for both configuration "A" and "B" in a wide variety of blowing ratios. At Re =10k, configuration "B" performed much better than configuration "A". This may be due to the interaction of the opposing jets in B having a larger influence on the cross flow in the main channel as opposed to the offset jets used in configuration "A" .

At 25,000 Reynolds numbers, both configurations performed well and both experienced a dip in values with blowing ratios near 15:1. This "dip" may be due to the location of the flow reattachment and recirculation points having an optimal set of parameters to cause high turbulence at BR near 10-12 (akin to the in pressure waves in an open pipe) and an turbulence cancelling effect at BR near 14-15. Multiple tests were performed using the B configuration near the 10 and 15 blowing ratio values to see if this anomaly could be repeated and explained. The results in figure 7 show that repeated testing provided similar results. The data points for all Reynolds numbers presented indicate this same trend on a less prominent scale. Trip strips used in traditional turbine blade internal passages show some tendency for this to occur, but not to the extent shown at Re=25k in this series of tests. A possible explanation for this may be that trip strips are a defined obstruction and have a set pitch, while the high velocity jets do not have a defined height and the width of the jet increases as it crosses the main channel flow path. Also, the traditional trip strip size and shape is unaffected by the main channel flow, while the jet flow can be severely altered or destroyed as the jet flow crosses the main channel.

As the Reynolds number increases the increased momentum of main channel fluid overcomes the momentum of fluid coming from each individual jets at lower blowing ratios and tends to direct the fluid leaving the jet downstream. The

effect of the opposing jets interacting to increase turbulence is reduced at these lower blowing ratios.

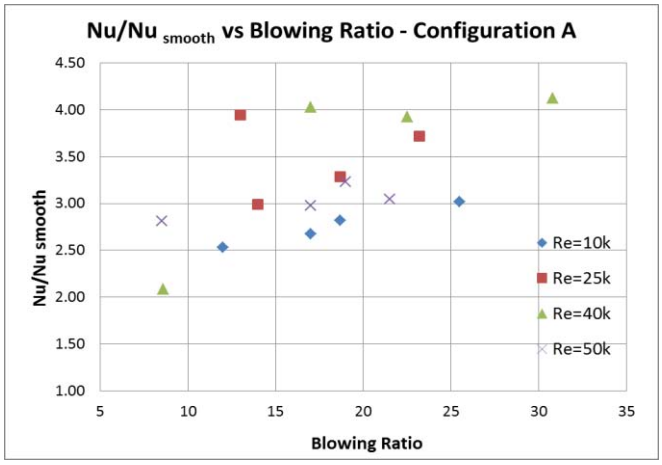

FIGURE 8: HEAT TRANSFER ENHANCEMENT VALUES FOR CONFIGURATION A.

The Re= 40k tests performed the best in configuration "A" with several Nu/Nu $_{smooth}$ values near or above 4.0 in all of the higher blowing ratios tested. In the B configuration the Re = 40k tests were nested in the mid-range of all tests performed in the "B" configuration. The offset jets in configuration "A" are the likely reason for the exceptional performance. Overall, the "A" configuration tests were better performers when compared to the "B" configuration tests.

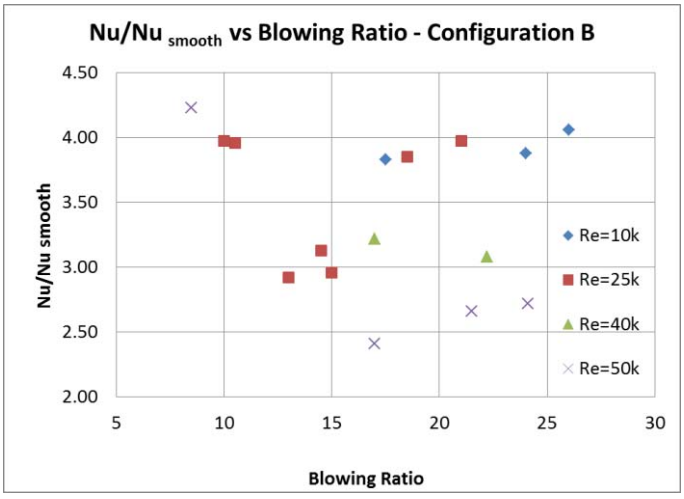

FIGURE 9: HEAT TRANSFER ENHANCEMENT VALUES FOR CONFIGURATION B.

The normalized friction factor for all the swirl-jet cases are relatively low for all cases tested when compared to published data employing trip strips in rectangular channels, which are typically found to be in the 5-10 range for turbulated channels of turbine blades. The various swirl-jet case plots appear to be insensitive to Reynolds numbers and ranged from ~1.0 to 2.7. It should be noted that the friction factor for the tests utilizing the jet enhancements is a combination of friction factors in the main channel and two outer jet supply channels (Eq. 6).

Equation 8 is used to determine the thermal performance of each test. It is important to note that the values of Nu are an area averaged value that takes into account one entire side of the test section between entry and exit pressure taps, not just the developed region.

$$\text{OTP} = \frac{Nu}{Nu_{o\ smooth}} \div \left(\frac{f_{total}}{f_{o\ smooth}}\right)^{1/3} \quad (8)$$

A plot of the calculated values summarizes the results in figure 10 for the "A" configuration jets and figure 11 for the "B" configuration jets. As expected from the previous plots, the jet configuration "A" performs extremely well at blowing ratios above 10 and extremely well at Re= 25k and Re = 40k. It should be noted that typical values reported in the literature for turbulated channels range between 1-1.5, and values higher than 1.5 are considered to be very good configurations for enhancing heat transfer without the associated friction penalty [13]. The swirl-jet configurations tested here lead to numbers in the 1.5-3.5 range, with the vast majority of tests yielding values in the 2.5 to 3.5 range, over a reasonable Reynolds numbers of 10,000-50,000. These configurations should therefore be considered promising.

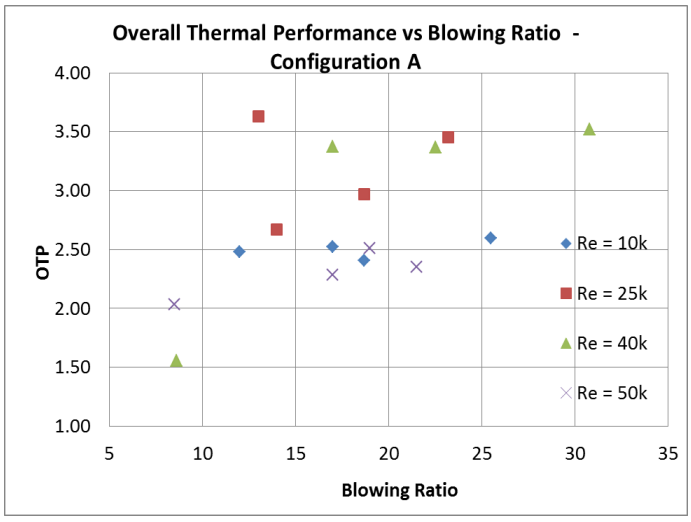

FIGURE 10: OVERALL THERMAL PERFORMANCE VALUES FOR CONFIGURATION A.

Configuration "B" also showed very good OTP values for the Re = 10k, 25k, and 40k tests. The tests performed at

Re=50k, at high blowing ratios, were some of the lowest performers with values between 2.0 and 2.25.

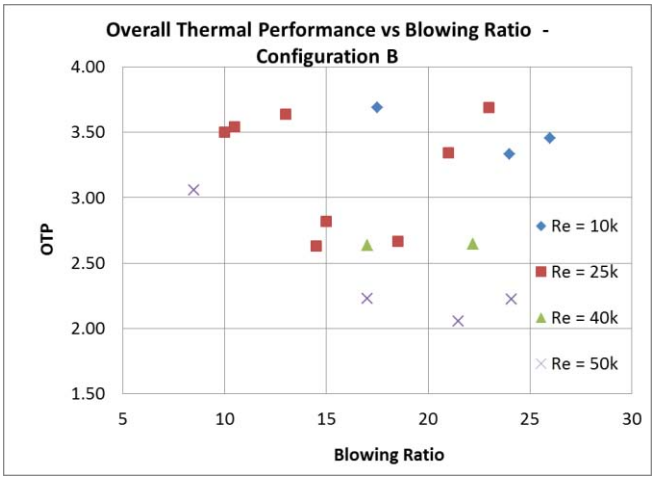

FIGURE 11: OVERALL THERMAL PERFORMANCE VALUES FOR CONFIGURATION B.

Jet velocities play an important role in swirl-enhancement. As blowing ratios and Reynolds numbers increased, so did the average exit velocity in the jets.

Configuration A			Configuration B		
Re x 10^{-3}	B.R.	Jet Vel. (m/s)	Re x 10^{-3}	B.R.	Jet Vel. (m/s)
10	12	62	10	17.5	79
10	17	77	10	24	93
10	18.7	83	10	26	102
10	25.5	99	25	10	120
25	13	141	25	10.5	133
25	14	169	25	13	141
25	18.7	208	25	14.5	175
25	23.2	255	25	15	178
40	8.6	192	25	18.5	205
40	17	290	25	21	223
40	22.5	329	25	23	252
40	30.8	343	40	17	290
50	8.5	207	40	22.2	327
50	17	312	50	8.5	207
50	19	321	50	17	312
50	21.5	329	50	21.5	329
			50	24.1	337

TABLE 3: AVERAGE JET EXIT VELOCITY VALUES FOR CONFIGURATIONS A AND B.

Table 3 summarizes the velocity for each combination of tests. The jet exit velocities ranged from a low of 62 m/s to a high of 343 m/s as the blowing ratios spanned values of 8.6 to 30.8. These are average jet velocities. In a typical low blowing ratio tests the jet velocity would drop by 3- 5 m/s from the first jet to the last. In the highest blowing ratio tests the jet velocity would reduce by as much as 18 m/s from the first jet to the last jet. Table 3 shows the average jet velocity for each test. The higher temperatures and higher pressures contributed to a choke velocity of 367 m/s. Therefore, the jets did not encounter a choke condition during these series of tests.

Heat Transfer Contour Plots

For comparison purposes Nu/Nu_o plots of the slot shaped channel with a 12.5 mm radiused entry and air entering thorough a straight entry is shown in figure 12. The Nu/Nu_o values are 1.04, 1.11, 1.28, and 1.32 for Re=10k, 25k, 40k, and 50k respectively. Every effort was made to have the scale values of the Nu/Nu_o plots the same for each series of tests. In most cases however, in order to achieve the best definition and contrast in Nu/Nu_o plots the scales could not be the same.

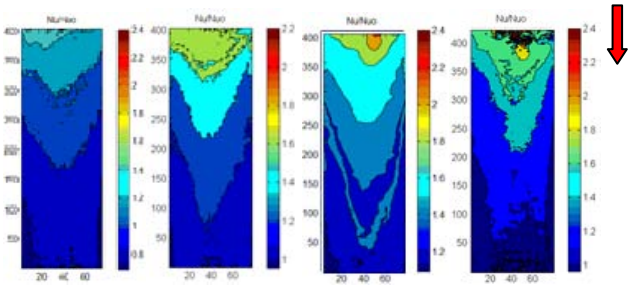

FIGURE 12: Nu/Nu_o PLOTS FOR THE SLOT SHAPED CHANNEL WITH A STRAIGHT ENTRY FOR Re=10k, 25k, 40k, AND 50k RESPECTIVELY.

Jet-Swirl Configuration "A":

This series of test examined the heat transfer enhancement characteristics when high blowing ratio jets were introduced into the main channel flow. Reynolds numbers ranged from 10,000 to 50,000. The diameter of each jet was 1.6 mm and provided an effective p/d ratio of 12:1, which is a commonly used ratio in the trip strip tests [8, 9]. The b/d ratio was 0.1. Air enters the main channel through two separate paths. One end of the slot shaped channel is connected to a diffuser from which the initial main channel air enters. Additionally, tangential side jets introduce air through neighboring channels. The offset of jet on any single side of the test piece is 38 mm. Jet holes on the opposite side are staggered by 19 mm. Details of configuration "A" is shown in figure 3.

Figure 13 shows the Nu/Nu_o plots of jet configuration "A" at an equivalent total mass flow to that of a Re = 10k, 25k,

& 40k, respectively, in the smooth non-enhanced slot shaped channel with a blowing ratio of 17. The jets on the opposing side are staggered in relation to the jets as shown in figures 3. At Re = 10k, the jet flow impinges on the surface of the main channel and cause very high local heat transfer enhancement, up to twelve in the main channel entry region. The enhancement values adjacent to each jet stream are much lower, especially near the entry, but as the flow proceeds through the channel the mixing quality improves with increasing crossflow, and there exists a more even distribution of heat transfer enhancement along with high local impingement values. The jet flow tends to cause swirl motion of the jet fluid and the main stream fluid seems to tumble as it encounters the high velocity jet fluid.

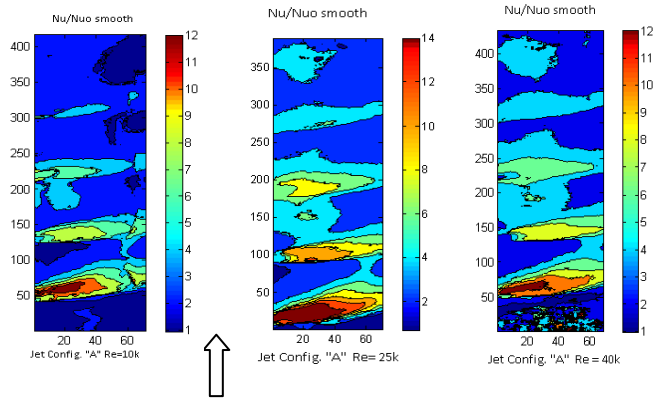

FIGURE 13: $Nu/Nu_{o\ smooth}$ JET CONFIGURATION "A", Re=10k, 25k, & 40k, w/ B.R. = 17

The combination of swirl and tumble leads to the high heat transfer enhancement in this configuration. It is important to note that the jets continue to add mass into the main channel as the fluid progresses from the entry to the exit and that the total mass does not equal to mass flow rate of the Re=10k flow of the smooth channel until near the exit of the channel. This explains why the enhancement levels are higher at the channel inlet where the local channel flow rate and average velocity are the lowest along the length of the channel. Therefore the local jet to channel flow velocity ratio is the highest at this entry location.

At a Reynolds number of 25k and 40k, figure 13 displays similar attributes to those discussed for Re = 10k. Large local areas with Nu/Nu_o values exceeding 4 are noted throughout the channel and continue to the channel exit. At Re=25k, for example, the overall mean thermal performance value is 2.97 with a Nu/Nu_o value of 4.05. The normalized friction factor remains low at 1.87. These values offer a significant improvement over the helical trip strips and most other published data related to heat transfer enhancement in the mid-span region of turbine blades.

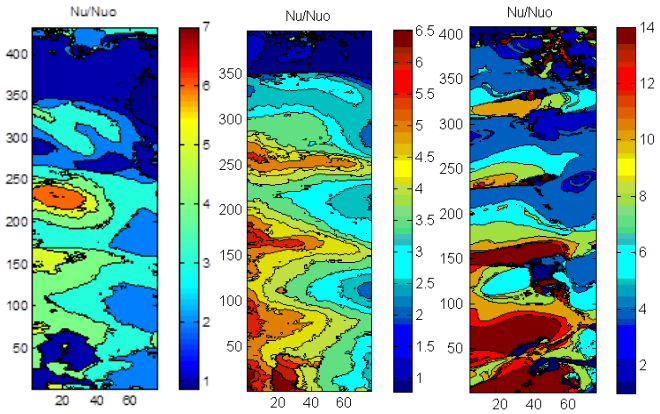

FIGURE 14: Nu/Nu_o JET CONFIGURATION "A", Re=10k, w/ B.R. = 12, 18.7, 25.5

Figure 14 shows the Nu/Nu_o color contour plots for jet configuration "A", an equivalent Reynolds number of 10,000 and three different blowing ratios. The center plots, BR = 18.7 displays the overall best heat transfer distribution and yields an overall thermal performance value of 2.41. The overall thermal performance value for the 25.5 blowing ratio was slightly higher, at 2.60, but the distribution is not as uniform.

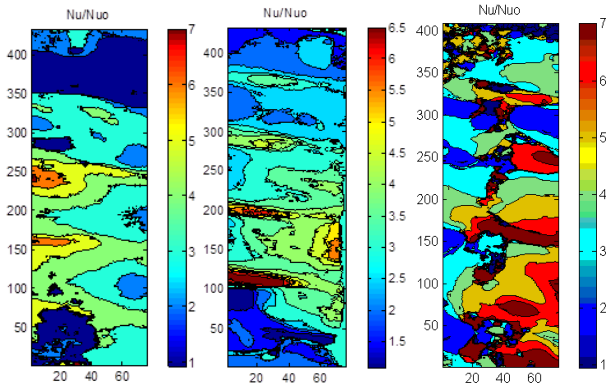

FIGURE 15: Nu/Nu_o JET CONFIGURATION "A", Re=25k, w/ B.R. = 14, 18.7, 23.2

As the effective Reynolds number increased the OTP values increased. In figure 15 three blowing ratio color plots are shown. The highest blowing ratio provided the best OTP value of 3.46 along with highly turbulent regions throughout the channel. The 18.7 blowing ratio plot had an OTP of 2.97. The lower blowing ratio plot appears to have a large section of low heat transfer which severely affect the overall thermal performance.

Good heat transfer distribution is observed in the high blowing ratio color plots in figure 16. At Re = 40k the increasing main channel velocity interacts with the high velocity side jets to provide the best overall heat transfer distribution of any of the tests performed.

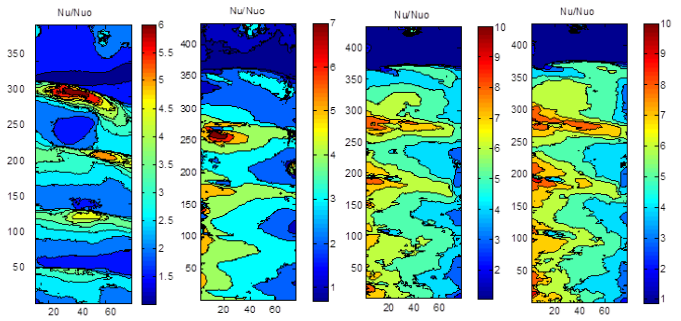

FIGURE 16: Nu/Nu$_o$ JET CONFIGURATION "A" , Re=40k, w/ B.R. = 8.6, 13, 22.5, 30.8

The normalized Nusselt number is 4.13 for the 30.8 blowing ratio tests and the OTP value is 3.52. The 22.5 blowing ratio tests displayed similar results with a normalized Nusselt value of 3.92 and an OTP of 3.37. The OTP values for the BR = 13 and the BR = 8.6 tests were 3.37 and 1.55 respectively.

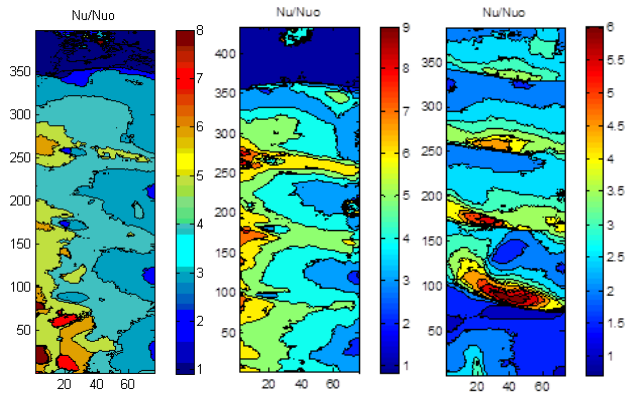

FIGURE 17: Nu/Nu$_o$ JET CONFIGURATION "A" , Re=50k, w/ B.R. = 21.5, 19, 8.5

The Re=50k tests yielded OTP results that were similar (see Figure 17). At BR = 21.5 the OTP was 2.35, while the results of BR = 19 were 2.51, and the BR = 8.5 tests showed an OTP value of 2.03. The distribution was generally good for all tests performed at Re = 50k.

Jet-Swirl Configuration "B":

The jet layout in configuration "B" is shown in figure 3. The spacing between jets was the same as configuration "A", at 38 mm, but the opposing jets were directly across from one another. Whereas the jets in configuration "A", in an idealized fashion, caused the jets to create a continuous helical swirl as the high velocity jets of air proceeding through the main channel, the jets in configuration "B" caused the jets to cross one another on opposite walls of the main channel. Therefore, the patterns of heat transfer distribution are somewhat different.

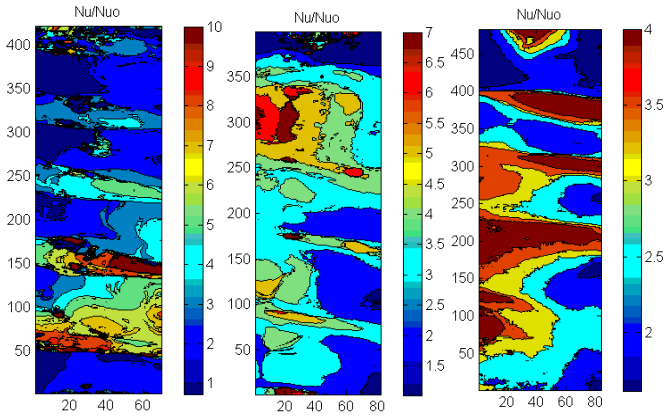

FIGURE 18: Nu/Nu$_o$ JET CONFIGURATION "B" , Re=10k, w/ B.R. = 17.5, 24, 26

Figure 18 displays the color contour plots of 10,000 Reynolds number tests with high blowing ratios of 17.5, 24, and 26 respectively. The overall thermal performance values are 3.69, 3.33, and 3.46 respectively. These values are very high, but the heat transfer distribution is not very good.

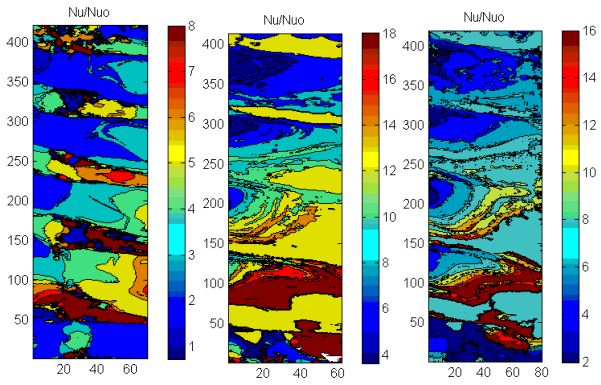

FIGURE 19: Nu/Nu$_o$ JET CONFIGURATION "B" , Re=25k, w/ B.R. = 13,15, 21

Increasing the Reynolds number to 25,000 helped the distribution and provided good overall thermal performance values of 3.64 for BR = 13, 2.82 for BR = 15, and 3.34 for BR = 21 (see Figure 19). The pressure losses for the BR = 15 tests were slightly higher than the other two tests. This contributed to the lower OTP value.

CONCLUSION

A series of tests were performed to determine heat transfer enhancement characteristics of a slot shaped channel, with jets issuing from side channels, using two different jet configurations and a multitude of blowing ratios. The resulting values of overall heat transfer enhancement, normalized friction

factors, and overall thermal performance were compared to a smooth slot employing no enhancements.

The jet configurations show a substantial improvement in mean heat transfer enhancement values when compared to published results for mid-span cooling techniques which usually utilize trip strips. Configuration "A" in this study shows extremely good values for overall thermal performance with a value of 3.63 at a Reynolds number of 25,000 and a blowing ration of 13. Configuration "B" also performed well with the maximum overall thermal performance value of 3.69 at a Reynolds number of 25,000 and a blowing ratio of 23.The normalized friction factor remained below 2.5 for all tests using jet enhancements. Generally, the higher the blowing ratios resulted in better overall heat transfer distribution in the channel for jet configuration "A". Jet configuration "B" did not show an even heat transfer distribution in most tests.

This test setup may not directly translate to a flow path in a turbine blade, but the concepts and unique features can be applied to current designs.

ACKNOWLEDGEMENTS

The authors wish to thank the Clean Power and Energy Research Consortium for funding this project. We also would like to acknowledge Brunet Breaux for his assistance in conducting many of the tests, Dr. Yi Liang for his assistance with the Matlab computer programming used to analyze the test results, and Norbert Sigue for fabricating many of the components used in the tests.

REFERENCES

[1] Wagner, J. H., Johnson, B. V., Graziani, R. A. and Yeh, F. C., 1992. "Heat Transfer in Rotating Serpentine Passages with Trips Normal to the Flow". *J. Turbomachinery*, Trans. ASME, **114**, pp. 847-857.

[2] Glezer, B., Moon, H. K., Kerrebrock, J., Bons, J., and Guenette, G., 1998. "Heat Transfer in a Rotating Radial Channel with Swirling Internal Flow". ASME Paper 98-GT-214.

[3] Hedlund, C. R., Ligrani, P. M., Moon, H. K., and Glezer, B., 1998. "Heat Transfer and Flow Phenomena in a Swirl Chamber Simulating Turbine Blade Internal Cooling". ASME Paper 98-GT-466.

[4] Bunker, R.S. , 2004. "Latticework (Vortex) Cooling Effectiveness Part 1: Stationary Channel Experiments". ASME Paper No. GT-2004-54157.

[5] Goreloff, V., Goychengerg, M., and Malkoff, V., 1990. "The Investigation of Heat Transfer in Cooled Blades of Gas Turbines". *26th Joint Propulsion Conference*. AIAA Paper No. 90-2144.

[6] Acharya, S., Zhou, F., Lagrone, J., Mahmood, G. and Bunker, R.S., 2005. "Latticework (Vortex) Cooling Experiments: Rotating Channel Experiments". *Journal of Turbomachinery*, **127**, pp. 471-478.

[7] Gillespie, D., Ireland, P. T., and Dailey,G. M., 2000. "Detailed Flow and HeatTransfer Coefficient Measurements in a Model of an Internal Cooling Geometry Employing Orthogonal Intersecting Channels". ASME Paper No. 2000-GT-653.

[8] Lei Wang, Bengt Sunden, 2007. "Experimental Investigation of Local Heat Transfer in a Square Duct with Various-shaped Ribs". *Heat Mass Transfer*, **43**, pp. 759-766.

[9] Taslim, M.E., Li, T., Kercher, D.M., 1996. "Experimental Heat Transfer and Friction in Channels Roughened With Angled, V-Shaped, and Discrete Ribs on Two Opposite walls". *Trans. ASME, Journal of Turbomachinery*, **118**, pp. 20-28.

[10] İrfan Kurtbaş, 2009. "Heat transfer augmentation by swirl generators inserted into a tube with constant heat flux". *International Communications in Heat and Mass Transfer*, **36**, pp. 865–871.

[11] Glezer, B., Moon, H. K., Kerrebrock, J., Bons, J., and Guenette, G., 1998. "Heat Transfer in a Rotating Radial Channel with Swirling Internal Flow". ASME Paper 98-GT-214.

[12] C.R. Smith, D.R. Sabatino, and T.J. Praisner, 2001. "Temperature sensing with thermochromic liquid crystal". *Experiments in Fluids*, **30**, pp. 190-201.

[13] G. Tanda, 2004. "Heat transfer in rectangular channels with transverse and V-shaped broken ribs". *International Journal of Heat and Mass Transfer*, **47**, pp. 229–243.

